

# Modeling Anisotropic Stress-Strain Response and Crystallographic Texture Evolution in $\alpha$ -Titanium during Large Plastic Deformation using Taylor-Type Models: Influence of Initial Texture and Purity

XIANPING WU, SURYA R. KALIDINDI, CARL NECKER, and AYMAN A. SALEM

The anisotropic strain-hardening behavior and texture evolution during large plastic strains were investigated in two different grades of  $\alpha$ -titanium. A recently proposed Taylor-type crystal-plasticity model<sup>[1]</sup> was used to predict the crystallographic texture evolution and anisotropic stress-strain response of these materials during large plastic strains at ambient temperature. The reasonable agreement between the predictions and the measurements reported here demonstrates the potential of these models for a class of titanium alloys in which plastic deformation is accommodated by both crystallographic slip and deformation twinning. The results of this study also provided quantitative insights into the effects of purity level on the slip and twin-hardening parameters, which are also observed to be relatively insensitive to the initial texture in the sample.

DOI: 10.1007/s11661-008-9651-x

© The Minerals, Metals & Materials Society and ASM International 2008

## I. INTRODUCTION

A number of studies<sup>[2-5]</sup> have observed that deformation twinning is an important mechanism of plastic deformation, in addition to crystallographic slip, in several commercially important metals. Many of the hexagonal close-packed metals and the low stacking-fault energy cubic metals exhibit deformation twinning. The occurrence of deformation twins has been correlated to major changes in both the strain-hardening response and the crystallographic texture evolution in these materials.<sup>[6-10]</sup>

A crystal-plasticity modeling framework has been employed successfully in the literature to study plastic deformation in polycrystalline metals.<sup>[11-15]</sup> However, most of the prior work in this field has focused on materials that exhibit only crystallographic slip. Given the important role of deformation twinning in several commercially important metals, it is highly desirable to extend the current crystal-plasticity modeling framework to include deformation twinning as an additional mode of plastic deformation. There have been several reports in recent literature addressing the various

challenges involved in incorporating deformation twinning in crystal-plasticity models.<sup>[16-20]</sup>

Some of the outstanding challenges in the development of crystal-plasticity models for hexagonal metals include the following: (1) description of the slip and twin-hardening laws that account for the complex interactions between them, (2) an efficient method for capturing grain fragmentation caused by twinning, and (3) a suitable homogenization theory that can be used to predict the response of the polycrystals from the response of individual crystals. In our prior work,<sup>[1]</sup> we have formulated slip and twin-hardening laws for  $\alpha$ -Ti that were motivated by a series of experimental investigations, while accounting for several observed complex slip-twin interactions. We have also demonstrated that a Taylor-type crystal-plasticity model based on a new grain-fragmentation scheme provided reasonable predictions for both the anisotropic stress-strain curves and the averaged texture evolution in a high-purity  $\alpha$ -Ti sample subjected to a range of monotonic deformation paths. In this new fragmentation scheme, each grain\* was allowed to be fragmented into one

---

\*The constituent single crystals in a polycrystal are often referred to as grains.

---

parent and several offspring grains (one offspring grain corresponding to one potential twin system in the original grain). Once a grain is fragmented, the newly formed parent and offspring grains were treated as independent grains.

It should be noted that a number of alternative approaches to the Taylor-type models are being explored currently in the literature, including the self-consistent methods<sup>[17,21,22]</sup> and the finite-element models.<sup>[18,23]</sup>

---

XIANPING WU, Engineering Advisor, formerly with the ExxonMobil Research and Engineering Company, Annandale, NJ 08801, is with Smith Technologies, Houston, TX 77032. SURYA R. KALIDINDI, Professor and Department Head, is with the Department of Materials Science and Engineering, Drexel University, Philadelphia, PA 19104. Contact e-mail: skalidin@coe.drexel.edu. CARL NECKER, Technical Staff Member, is with the Metallurgy Group-MST-6, Los Alamos National Laboratory, Los Alamos, NM 87545. AYMAN A. SALEM, Technical Staff Member, is with the Materials Processing Laboratory, operated by UES Inc., AFRL/MLLM, Wright-Patterson AFB, OH 45433, and the Universal Technology Corporation, Dayton, OH 45431.

Manuscript submitted on January 26, 2008.

Article published online September 20, 2008

There have also been attempts to include grain-boundary sliding as a significant contributor to the plastic deformation in Mg alloys<sup>[24,25]</sup> However, it should be noted that grain-boundary sliding is not relevant to the Ti alloys studied here because there is no experimental evidence indicating that it is an important contributor to their plastic deformation at room temperature.

Building on our previous success, we conducted a new study to critically evaluate the accuracy of the Taylor-type model (with the newly formulated grain-fragmentation scheme) by applying it to a different grade of  $\alpha$ -Ti with a different initial texture. The sensitivity of the mechanical behavior of  $\alpha$ -titanium and its alloys to the initial texture and the impurity levels has been demonstrated *via* mechanical testing at a wide range of temperatures.<sup>[26]</sup> In our prior work,<sup>[1]</sup> we used high-purity  $\alpha$ -titanium (HP-Ti). In this work, we focus our attention on commercial-purity  $\alpha$ -titanium (CP-Ti). Compared to HP-Ti, CP-Ti is expected to exhibit much higher yield strength and substantially different strain-hardening characteristics. Moreover, the CP-Ti samples we obtained had significantly different starting textures compared to the HP-Ti sample. It was anticipated that the large differences in the starting textures between the HP-Ti and CP-Ti samples will serve to evaluate critically the predictive capability of our recently formulated Taylor-type crystal-plasticity model.<sup>[1]</sup>

## II. TAYLOR-TYPE CRYSTAL PLASTICITY MODELS FOR HEXAGONAL-CLOSE-PACKED METALS

The main details of the crystal-plasticity model used in this study are summarized in this section. Further details can be found in the literature.<sup>[1]</sup>

### A. Grains Prior to Fragmentation

The total deformation gradient on a crystalline region,  $\mathbf{F}$ , is decomposed into elastic and plastic components as follows:

$$\mathbf{F} = \mathbf{F}^* \mathbf{F}^P \quad [1]$$

where  $\mathbf{F}^*$  and  $\mathbf{F}^P$  represent the elastic and plastic deformation gradient, respectively. The elastic behavior of the single crystal is expressed as follows:

$$\mathbf{T}^* = \mathbf{C} [\mathbf{E}^*] \quad [2]$$

where  $\mathbf{C}$  represents the anisotropic fourth-rank elastic-stiffness tensor. The terms,  $\mathbf{T}^*$  and  $\mathbf{E}^*$ , are a pair of work-conjugate stress and strain measures defined as follows:

$$\mathbf{T}^* = \mathbf{F}^{*-1} \{ (\det \mathbf{F}^*) \mathbf{T} \} \mathbf{F}^{*-T} \quad [3]$$

$$\mathbf{E}^* = \frac{1}{2} \{ \mathbf{F}^{*T} \mathbf{F}^* - \mathbf{1} \} \quad [4]$$

where  $\mathbf{T}$  denotes the Cauchy stress in the crystalline region of interest. The evolution of the plastic deformation gradient is described by the following equations:

$$\dot{\mathbf{F}}^P = \mathbf{L}^P \mathbf{F}^P \quad [5]$$

$$\mathbf{L}^P = \sum_{\alpha}^{N^s} \dot{\gamma}^{\alpha} \mathbf{S}_o^{\alpha} + \sum_{\beta}^{N^{tw}} \dot{f}^{\beta} \gamma_{tw}^{\beta} \mathbf{S}_o^{\beta} \quad [6]$$

The two terms on the right-hand side of Eq. [6] represent the contributions to plastic deformation by crystallographic slip and deformation twinning, respectively. The terms  $\mathbf{S}_o^{\alpha}$  and  $\mathbf{S}_o^{\beta}$  denote the unit slip and twin tensors in the initial crystal orientation, respectively. The term  $\dot{\gamma}^{\alpha}$  represents the slip-shear rate on a slip system,  $\alpha$ . The term  $\dot{f}^{\beta} \gamma_{tw}^{\beta}$  represents the homogenized shear rate in the crystal due to deformation twinning. The term  $\gamma_{tw}^{\beta}$  denotes the amount of constant shear associated with twin system,  $\beta$ , and  $f^{\beta}$  denotes its volume fraction in the crystalline region of interest.

The evolution of plastic shearing rates on slip and twin systems is described by appropriate power laws, following the viscoplastic approach,<sup>[12]</sup> as follows:

$$\dot{\gamma}^{\alpha} = \dot{\gamma}_o \left| \frac{\tau^{\alpha}}{s^{\alpha}} \right|^{1/m} \text{sign}(\tau^{\alpha}) \quad [7]$$

$$\dot{f}^{\beta} = \begin{cases} \frac{\dot{\gamma}_o}{\gamma_{tw}^{\beta}} \left| \frac{\tau^{\beta}}{s^{\beta}} \right|^{1/m} & \text{if } \tau^{\beta} \geq 0 \\ 0 & \text{if } \tau^{\beta} \leq 0 \end{cases} \quad [8]$$

The rate-sensitivity parameter,  $m$ , in Eqs. [7] and [8] was set to a very low value of 0.02 in order to simulate the near rate-independent behavior of  $\alpha$ -Ti at ambient temperature. The reference slip rate,  $\dot{\gamma}_o$ , was set as  $0.001 \text{ s}^{-1}$  to reflect the quasi-static loading condition used in this study. The terms  $\tau^{\alpha}$  and  $s^{\alpha}$  represent the resolved shear stress and the shear resistance for a particular slip or twin system. The resolved shear stress for both slip and twin systems can be defined as follows:

$$\tau^{\alpha} \approx \mathbf{T}^* : \mathbf{S}_o^{\alpha} \quad [9]$$

A total of 18 slip systems belonging to three distinct slip families and 12 twin systems belonging to two distinct twin families were considered (Table I). The evolution of the slip and twin hardening is described phenomenologically by the following model:

$$\begin{aligned} \dot{s}^{\alpha} &= h_s^{\text{pri}} \left( 1 - \frac{s^{\alpha}}{s_s^{\alpha}} \right) \sum_k^{N_s^{\text{pri}}} |\dot{\gamma}^k| + h_s^{\text{bas}} \left( 1 - \frac{s^{\alpha}}{s_s^{\alpha}} \right) \sum_l^{N_s^{\text{bas}}} |\dot{\gamma}^l| \\ &+ h_s^{\text{pyr}} \left( 1 - \frac{s^{\alpha}}{s_s^{\alpha}} \right) \sum_m^{N_s^{\text{pyr}}} |\dot{\gamma}^m| \end{aligned} \quad [10]$$

$$\begin{aligned} h_s^{\text{pri}} &= h_{so}^{\text{pri}} \left( 1 + C \left( \sum_{\beta} f^{\beta} \right)^b \right), \quad h_s^{\text{bas}} = h_{so}^{\text{bas}} \left( 1 + C \left( \sum_{\beta} f^{\beta} \right)^b \right), \\ h_s^{\text{pyr}} &= h_{so}^{\text{pyr}} \left( 1 + C \left( \sum_{\beta} f^{\beta} \right)^b \right) \end{aligned} \quad [11]$$

**Table I. Summary of Modeling Parameters for Slip and Twin Systems**

Family	Slip Systems			Twin Systems	
	Prismatic $\langle a \rangle$	Basal $\langle a \rangle$	Pyramidal $\langle c + a \rangle$	Compressive	Tensile
Plane and direction	$\{10\bar{1}0\}\langle 11\bar{2}0 \rangle$	$\{0001\}\langle 11\bar{2}0 \rangle$	$\{10\bar{1}1\}\langle 11\bar{2}3 \rangle$	$\{11\bar{2}2\}\langle 11\bar{2}\bar{3} \rangle$	$\{10\bar{1}2\}\langle 10\bar{1}1 \rangle$
Number of systems	3	3	12	6	6
Initial resistance	$s_{so}^{pri}$	$s_{so}^{bas}$	$s_{so}^{pyr}$	$s_{tw}^{com}$	$s_{tw}^{ten}$
Slip hardening parameters	$h_{so}^{pri}, s_{so}^{pri}$	$h_{so}^{bas}, s_{so}^{bas}$	$h_{so}^{pyr}, s_{so}^{pyr}$	no hardening parameters	
Other parameters	$C, b, s_{pr}$			needed for twin systems	

$$s_s^\alpha = \begin{cases} s_{so}^{pri} + s_{pr} \left( \sum_{\beta} f^\beta \right)^{0.5} & \text{if } \alpha \in \text{prism slip systems} \\ s_{so}^{bas} + s_{pr} \left( \sum_{\beta} f^\beta \right)^{0.5} & \text{if } \alpha \in \text{basal slip systems} \\ s_{so}^{pyr} + s_{pr} \left( \sum_{\beta} f^\beta \right)^{0.5} & \text{if } \alpha \in \text{pyramidal slip systems} \end{cases} \quad [12]$$

In Eqs. [10] through [12],  $h_s^\alpha$  and  $s_s^\alpha$  represent the hardening rate and the saturation value associated with the slip system,  $\alpha$ , respectively. The terms  $h_{so}^\alpha$  and  $s_{so}^\alpha$  denote the initial hardening rate and saturation value in the absence of twinning. The terms  $C$ ,  $s_{pr}$ , and  $b$  are the hardening parameters that aim to capture phenomenologically the complex interactions observed between slip and deformation twinning in a series of experimental investigations.<sup>[10,26,27]</sup> The term  $\sum_{\beta} f^\beta$  denotes the total

twin-volume fraction in the grain. The rationale leading to the formulation of these slip-hardening laws is described in our earlier studies.<sup>[1,19]</sup>

### B. Criterion for Grain Fragmentation

When the accumulated twin-volume fraction in any grain reaches the predetermined saturation value (taken as 0.4 based on our prior work), that grain is fragmented into a parent grain (corresponding to the untwined regions) and several offspring grains corresponding to the dominant twin systems. These newly formed grains are allowed to undergo further deformation as independent grains, but twinning is no longer allowed in these grains.

### C. Grains After Fragmentation

After fragmentation, the newly formed parent and offspring grains are assumed to have the same values of the slip resistances and hardening parameters as the untwined regions in the original grain. Note that the slip systems in offspring grains have different orientations compared to those in the parent grain due to the lattice rotation caused by twinning. The evolution of slip resistance continues to be described by Eqs. [10] through [12].

The preceding constitutive description is for the local mechanical response of a single-crystal region in a polycrystalline  $\alpha$ -titanium sample. The response of the polycrystalline aggregate is obtained by invoking the

extended Taylor assumption<sup>[28]</sup> of uniform deformation through the entire polycrystal. It has been widely reported in literature that the Taylor assumption results in reasonable predictions of deformed textures in single-phase medium to high stacking-fault energy cubic metals,<sup>[13–15]</sup> although they tend to be significantly sharper compared to experiments. In prior work,<sup>[1,19]</sup> we have demonstrated that the Taylor model continues to provide reasonably accurate predictions of deformed textures for hexagonal metals, although the predictions are qualitatively less accurate than those for the cubic metals.

## III. MATERIALS AND EXPERIMENTAL PROCEDURES

Two grades of pure titanium were studied: (a) commercial-purity titanium (CP-Ti) Grade-2 and (b) high-purity titanium (HP-Ti). The chemical composition of both materials is summarized in Table II. The CP-Ti was received as a 33-mm rolled plate and was given a recrystallization heat treatment of 830 °C/2 h, followed by air cooling to produce equiaxed-grain structure with the average grain size of 35  $\mu\text{m}$ . The annealed CP-Ti showed a rolling texture with the (0001) poles perpendicular to the transverse direction and smeared between the rolling direction (RD) and normal direction (ND) (Figure 1(a)). The HP-Ti was received as a 12-mm clock-rolled disk and was given a recrystallization heat treatment of 537 °C/1 h, followed by water quenching to obtain an equiaxed-grain structure with a 30- $\mu\text{m}$  average grain size. The initial texture of the HP-Ti showed a fiber texture with the  $c$ -axes of many grains distributed at approximately 20 to 35 deg from the ND direction (Figure 1(b)).

In our previous study,<sup>[1]</sup> in order to characterize the anisotropy of strain hardening, we subjected samples of HP-Ti to two different deformation paths (simple compression and simple shear). In the present study, we took a different approach. We conducted simple

**Table II. Chemical Compositions (in wppm) of CP-Ti and HP-Ti Used in This Study**

Alloy	O	Fe	S	C	N	Al	Ti
CP $\alpha$ -Ti	810	970	9	196	80	1200	balance
HP $\alpha$ -Ti	95	1.3	3	7	11	<1.0	balance

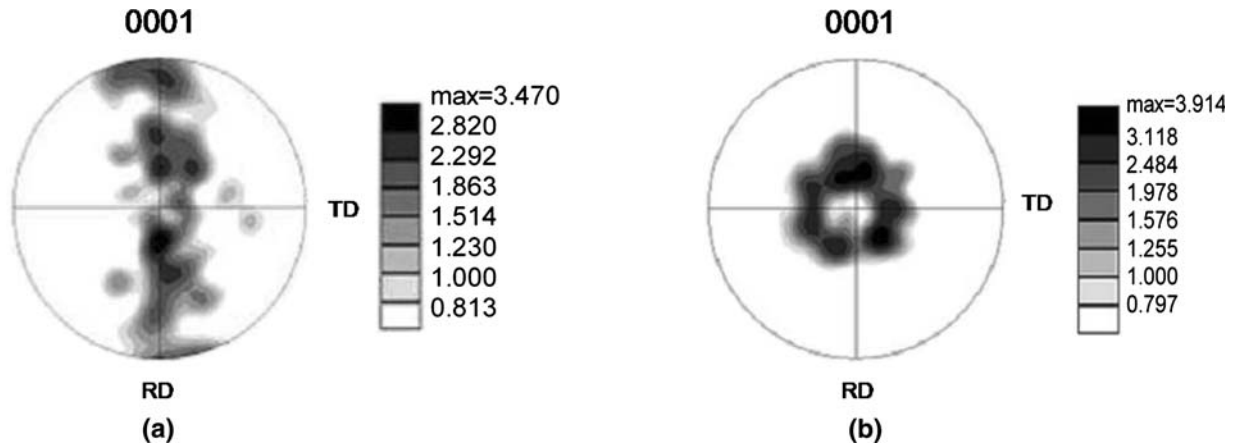


Fig. 1—Initial textures of the annealed samples: (a) CP-Ti and (b) HP-Ti.

compression tests on CP-Ti in three mutually orthogonal directions labeled as ND, TD, and RD. Because the annealed material has a strong initial texture, this approach is expected to give us substantially different stress-strain curves with different strain-hardening characteristics for the three tests. This dataset should be adequate to extract all of the strain-hardening parameters in the preceding model. Compression tests were conducted at room temperature on cylindrical samples at a constant strain rate of  $0.01 \text{ s}^{-1}$ . All specimens were lubricated using Teflon sheets and molybdenum disulfide ( $\text{MoS}_2$ ) to minimize the frictional effects. In addition, the compression tests were interrupted for relubrication at regular intervals of strain between 0.3 and 0.4. Load-displacement data were corrected for the compliance of the testing machine before calculating the true stress-true strain curves.<sup>[29]</sup>

The textures of the annealed samples were determined by the electron backscatter diffraction (EBSD) technique. For this purpose, specimens were sectioned, ground, and lightly electropolished at  $-20 \text{ }^\circ\text{C}$  in a solution of 590 mL methanol and 60 mL perchloric acid. Following electropolishing, the samples were mounted on the tilting stage inside an XL30 field-emission gun scanning electron microscope. The microscope was operated at 20 kV and 6 nA with the stage tilted at an inclination of  $70 \text{ deg}$ . The local Kikuchi patterns were collected and indexed using the EBSD system from EDAX. The textures of the deformed samples were determined from the measurements of  $(10\bar{1}0)$ ,  $(0001)$ ,  $(10\bar{1}1)$ ,  $(10\bar{1}2)$ ,  $(11\bar{2}0)$ , and  $(10\bar{1}3)$  pole figures using X-ray diffraction technique on a Scintag X1 5-axis pole figure goniometer using  $\text{Cu } K_\alpha$  radiation. The beam is point source, circularly collimated to 0.8 mm. The detector is a Peltier cooled solid-state detector with a slit of 2 mm. The samples had a minimum surface area of  $1.0 \text{ cm}^2$ . The samples were oscillated 4 mm to collect data from as many grains as possible. Data was collected out to 80-deg sample tilt in 5-deg sample rotation and tilt increments with a two-second counting time. The data was analyzed using the popLA software<sup>[30]</sup> to produce corrected and recalculated pole figures and orientation distributions.

#### IV. CALIBRATION OF TAYLOR-TYPE MODEL

In a previous study,<sup>[1]</sup> we established a procedure for estimating the model parameters by fitting the predicted stress-strain curves in two different deformation paths to the corresponding measurements. The same strategy was applied here for CP-Ti. In this study, the stress-strain curves in simple compression along ND and TD were used for calibration (Figure 2), and the measurement in simple compression along RD was used for evaluation (Figure 3).

For comparison, the values of model parameters for both CP-Ti and HP-Ti are summarized in Table III. The initial slip resistances ( $s_o^{\text{pri}}$ ,  $s_o^{\text{bas}}$ , and  $s_o^{\text{pyr}}$ ) in CP-Ti are twice their values in HP-Ti. It appears that the slip resistances of all the different slip systems scaled up by the same constant with increased levels of impurities in  $\alpha$ -Ti. It is also worth noting that this scaling factor of 2 also corresponds roughly to the average increase in the macroscopic yield strength between HP-Ti and CP-Ti (Figure 4). The resistance to twinning ( $s_{tw}$ ) in CP-Ti has increased by approximately three times compared to the twin resistance in HP-Ti, indicating that the increased impurities have a stronger influence on the twin resistance compared to the slip resistances. Note that the same parameters are used for tensile and compressive twins in the current model. The consequences of this simplification are discussed in Section VI-B. The initial slip-hardening rates ( $h_{s_o}^{\text{pri-bas}}$  and  $h_{s_o}^{\text{pyr}}$ ) in CP-Ti are an order of magnitude greater than those in HP-Ti. The initial slip-saturation values ( $s_{s_o}^{\text{pri}}$  and  $s_{s_o}^{\text{bas-pyr}}$ ) in CP-Ti are greater than those in HP-Ti. Both of these observations can be attributed to the fact that the impurities are expected to mitigate dynamic recovery. The slip-twin hardening parameter,  $s_{pr}$ , in CP-Ti is higher than that in HP-Ti by the same scaling factor of 2 discussed earlier. The slip-twin hardening parameter,  $C$ , showed a modest increase in CP-Ti, while the value of the parameter,  $b$ , remained the same. Needless to say, the trends seen here in the influence of impurities on the values of the various hardening parameters need to be validated with additional measurements in other grades of  $\alpha$ -Ti.

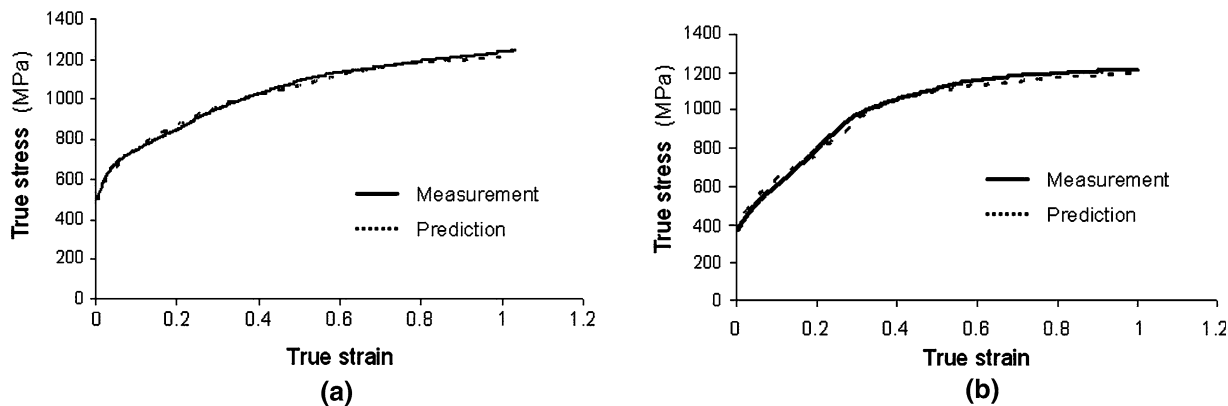


Fig. 2—Comparison of predicted and measured true stress–true strain curves in CP-Ti: (a) simple compression along ND and (b) simple compression along TD.

## V. EVALUATION OF TAYLOR-TYPE MODEL

After the model parameters were determined, the predictive capability of the proposed model was evaluated quantitatively by directly comparing the predictions to the measurements that were not used in the calibration process. The predicted stress-strain response in simple compression along RD showed good agreement with measurement (Figure 3). It is worth noting that the measured stress-strain curves (simple compression on CP-Ti along ND, TD, and RD) in Figure 4 show different features at an early stage (compressive strains lower than approximately 0.20); whereas, they approach each other and become similar at larger strains. These features are captured very well by the

model and are further supported by the texture measurements.

The texture measurements in the deformed samples were not used in the calibration of the hardening parameters, and, hence, they are used to evaluate the predictive capabilities of the model. All textures were rotated to position the loading directions in the center of each pole figure. In other words, the initial textures in these compression tests can be related to each other by simple rotations. In particular, the initial texture for TD compression is quite distinct from the initial textures for the other two compression tests (Figure 5). However, after a true strain of 1.0, all deformed textures are surprisingly similar to each other and are comprised of

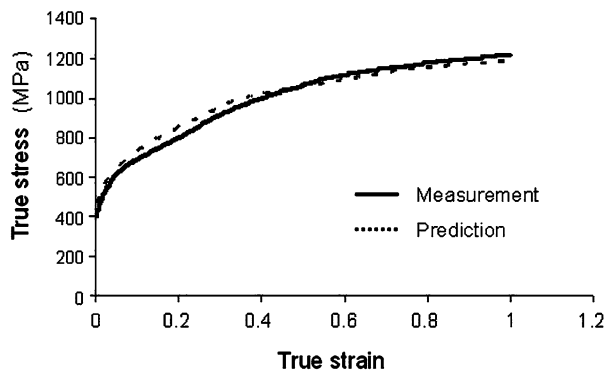


Fig. 3—Comparison of the predicted and measured stress-strain curves in simple compression test along RD for CP-Ti.

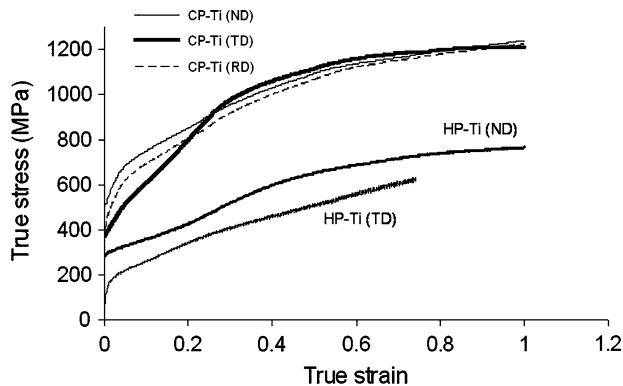


Fig. 4—Measured true stress–true strain curves in simple compression tests on CP-Ti and HP-Ti.

Table III. Summary of Estimated Model Parameters for  $\alpha$ -Ti

Parameter	$s_o^{\text{pri}}$	$s_o^{\text{bas}}$	$s_o^{\text{pyr}}$	$s_{tw}$	$h_{so}^{\text{pri-bas}}$	$h_{so}^{\text{pyr}}$
CP-Ti	60 MPa	300 MPa	240 MPa	400 MPa	800 MPa	1500 MPa
HP-Ti	30 MPa	150 MPa	120 MPa	125 MPa	15 MPa	300 MPa
Parameter	$s_{so}^{\text{pri}}$	$s_{so}^{\text{bas-pyr}}$	$s_{pr}$	$C$	$b$	—
CP-Ti	250 MPa	430 MPa	200 MPa	30	2	—
HP-Ti	100 MPa	300 MPa	100 MPa	25	2	—

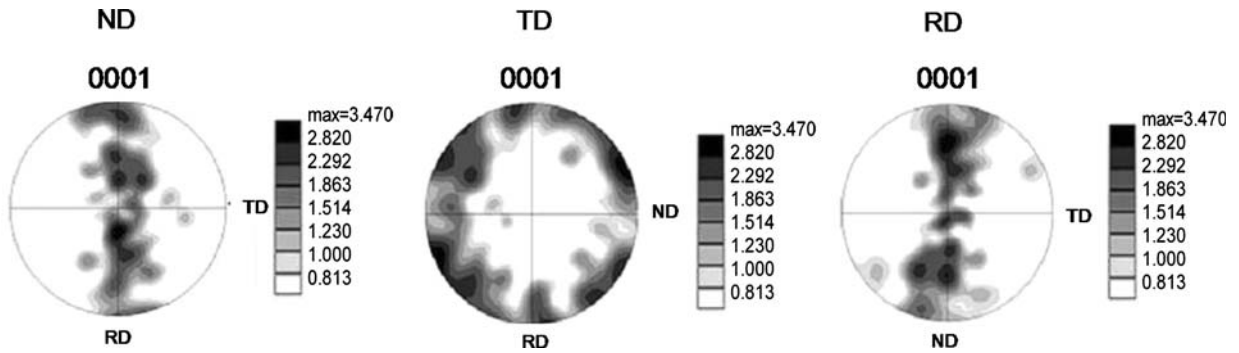


Fig. 5—Initial textures of CP-Ti samples in simple compression test along ND, TD, and RD.

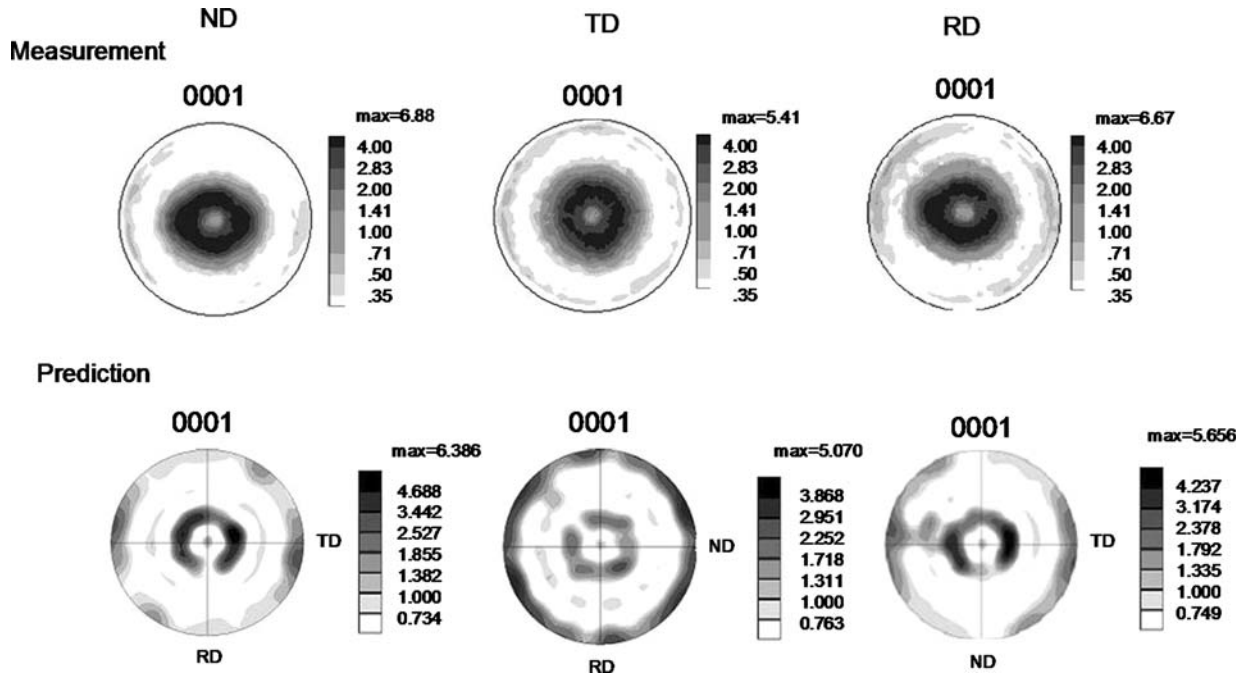


Fig. 6—Comparison of measured and predicted textures of CP-Ti at  $\epsilon = -1.00$  in simple compression tests along ND, TD, and RD, respectively.

two main components: (1) a strong fiber component with the  $c$ -axis approximately 10 to 30 deg from compression direction, and (2) a weak fiber component with the  $c$ -axis approximately 80 to 90 deg from compression direction. The predicted textures at large strain ( $\epsilon = -1.00$ ) in all the three compression tests showed reasonable agreement with measurement (Figure 6).

## VI. DISCUSSION

### A. Strain Hardening

The model parameters presented in Table III are important to understanding the strain-hardening response of  $\alpha$ -Ti during large deformation. Figure 4 clearly shows that CP-Ti exhibits a higher yield strength (attributed to the higher impurity content) compared to HP-Ti. More interestingly, there are indeed distinct differences in the initial portions of the stress-strain

curves from the three different compression tests (in three orthogonal directions) on CP-Ti. Surprisingly, these differences attenuate substantially after a moderate strain of only approximately 0.3. The stress-strain curve of HP-Ti (RD) was not available from the previous study. However, the HP-Ti sample has a strong initial fiber texture along ND, and, therefore, the stress-strain response of HP-Ti (RD) is expected to be very similar to that of HP-Ti (TD).

In our previous studies,<sup>[26,27]</sup> a normalized strain-hardening plot was used to identify the role of deformation twinning in the evolution of strain hardening for HP-Ti. In these plots, the strain-hardening rate normalized by shear modulus was plotted against the increment in yield stress due to cold work normalized by shear modulus. These plots revealed that the strain-hardening response of materials that exhibit deformation twinning can be divided into three stages for hexagonal-close-packed (hcp) metals.<sup>[27]</sup> The three stages in hcp metals

can be described as (a) a decreasing strain-hardening rate stage (stage A), corresponding to the deformation prior to the onset of twinning; (b) an increasing strain-hardening rate stage (stage B), corresponding to the initiation and growth of twinning; and (c) a decreasing strain-hardening rate stage (stage C), corresponding to the deformation after the saturation of twinning. The measured strain-hardening responses for CP-Ti studied also exhibit these same characteristics. For comparison, the strain-hardening curves for both HP-Ti and CP-Ti are plotted in Figure 7. The strain-hardening rates in CP-Ti at a given normalized stress are clearly higher than those in HP-Ti, which can be attributed to inhibition of dynamic recovery due to presence of impurities. The compression of CP-Ti along TD revealed a lower initial yield strength (Figure 4). However, the strain hardening caused by twinning in stage B produces a higher hardening rate in this sample compared to the other two compression tests on CP-Ti (Figure 7). Consequently, the flow stress rises to the values that are comparable to the flow stresses achieved in the compression tests in the other two directions. The initial texture and the subsequent twinning activity can explain the different behavior during CP-Ti compression along the TD direction. In particular, at the beginning of loading the TD sample, the *c*-axes of most grains were inclined close to 90 deg to the loading direction (Figure 5), and, hence, the sample exhibits a relatively low initial yield strength. After some strain, however, almost all grains exhibited tensile twinning. Consequently, the strain-hardening rate showed a rapid increase due to twinning. On the other hand, the materials that were loaded along the RD and ND directions had many grains with the *c*-axes close to the loading direction (Figure 5). Therefore, the deformation exhibited a higher initial yield strength (Figure 4). Further loading along the RD and ND directions caused several grains to twin but at a much lower rate. Therefore, the increase in the strain-hardening rate in stage B for RD and ND directions was less than that for the sample loaded along the TD direction. Upon twin saturation, all three samples reached similar flow stresses (Figure 4).

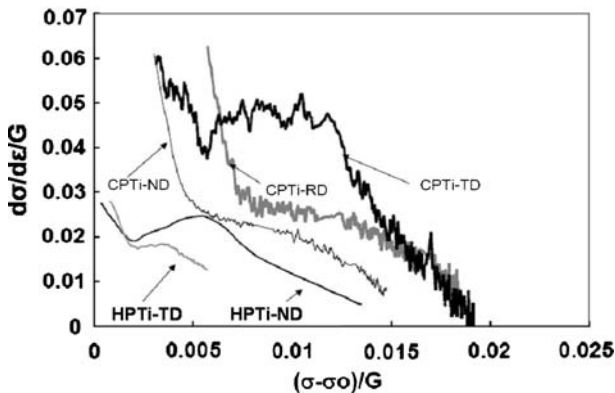


Fig. 7—Comparison of strain-hardening behaviors in simple compression of CP-Ti and HP-Ti samples. The ordinate is the normalized slope of stress-strain curve, and the abscissa is the normalized plastic-flow stress. The term,  $G$ , is the theoretical shear modulus of titanium and  $\sigma_0$  is the initial yield stress.

## B. Compressive and Tensile Twins

It has been reported earlier<sup>[23]</sup> that different twin families (*i.e.*, tensile and compressive twins) have distinctly different twin resistance. In our models, it was assumed that all the twin systems exhibit identical twin resistance. It is our intuition that allowing for different twin resistances will improve the predictive capabilities of our model. For example, it is observed in Figure 4 that simple compression along TD exhibits a lower yield strength but a higher strain-hardening rate compared to the samples compressed along ND and RD directions. This is also supported by the strain-hardening plots in Figure 7 where the strain-hardening rate in stage B of the TD compressed sample is much higher than the others. Due to the initial texture and twin orientations, it is anticipated that the twinning associated with the TD compressed sample will be mainly tensile twins ( $\{10\bar{1}2\}\{10\bar{1}1\}$ ); whereas, the twinning associated with the other samples will be mainly compressive twins ( $\{11\bar{2}2\}\{11\bar{2}\bar{3}\}$ ). Refinement of the hardening relations to allow for the differences between the resistances of the tensile and compressive twin systems should improve the predictive capability of the model described here.

## C. Twin Volume Fraction

Figure 8 shows the predicted twin volume fraction as a function of strain during simple compression of CP-Ti along ND, TD, and RD directions. It is clearly seen that the twinning associated with simple compression along TD is mainly tensile twins; whereas, the compressive twins dominate during simple compression along ND and RD. In addition, twin volume fraction associated with simple compression along TD is much higher than ND and RD at small strains, while the twin volume fractions become similar eventually for all directions at large strains. These modeling predictions support our proposed theory for the texture evolution and strain-hardening response revealed by Figures 5 through 7. A micrograph from orientation image microscope (OIM) measurement is presented in Figure 9 for the CP-Ti sample subjected to simple compression along ND at a strain of 0.22.<sup>[31]</sup> Using the line-intersection method, the area fractions of compressive and tensile twins are estimated to be approximately 9.0 and 1.1 pct, respectively. In comparison with the predictions in Figure 8, the measurement of compressive-twin volume fraction is significantly larger; whereas, the measurement of tensile-twin volume fraction is in good agreement. Note that a number of two-dimensional section measurements using much larger scan areas would be required in order to estimate accurately the twin volume fraction in the deformed sample. We plan to undertake such detailed characterization studies of twin volume fractions in future work.

## D. Homogenization Method

The model presented here employs the Taylor assumption of uniform deformation gradient in all of the crystals. It is well known that the Taylor model predicts

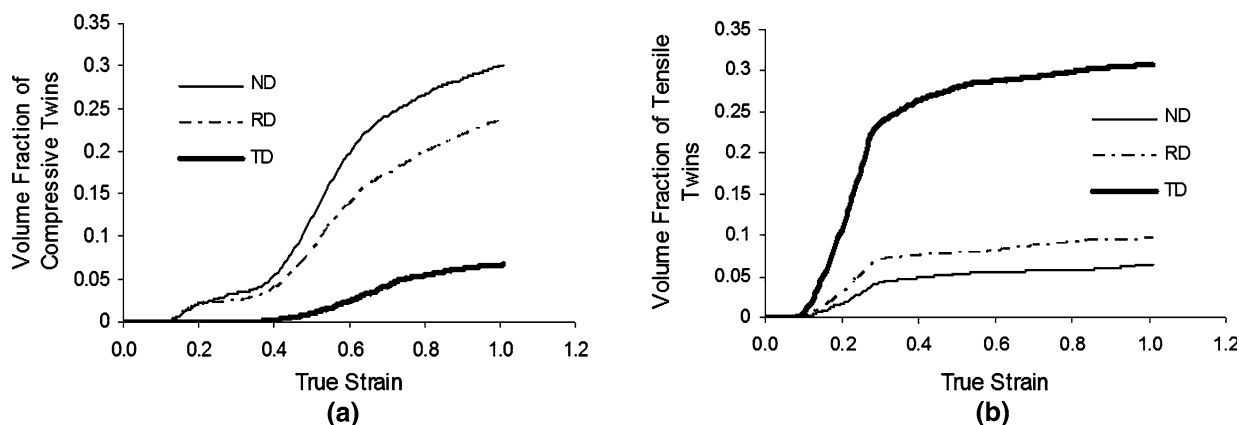


Fig. 8—Predicted volume fractions of (a) compressive and (b) tensile twins as a function of strain for CP-Ti samples in simple compression tests along ND, TD, and RD, respectively.

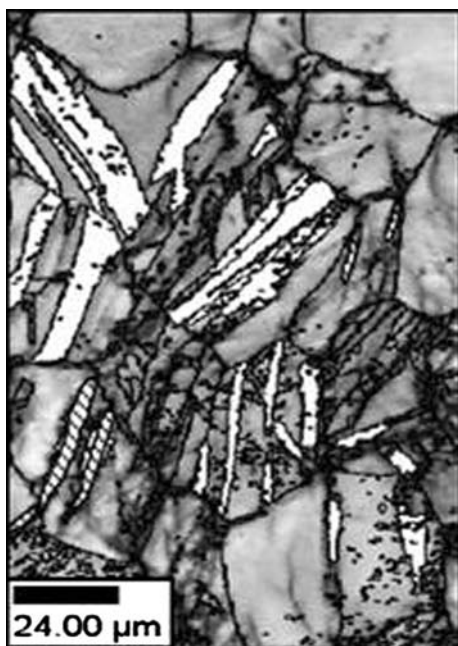


Fig. 9—OIM-reconstructed microstructures of CP-Ti at room temperature after  $-0.22$  true strain in simple compression along the ND direction (horizontal direction in the micrograph). The white areas are compressive twins, and the cross-hatched areas are tensile twins.

much stronger deformation textures for cubic metals compared to the experiments.<sup>[13–15,32]</sup> The same is also true for the  $\alpha$ -Ti studied here. It is clearly evident from the results presented that the Taylor-type model predictions for  $\alpha$ -Ti are not as accurate as they were for cubic metals. There is, therefore, a clear need to explore high-order homogenization theories in future studies.<sup>[18,23,33]</sup>

## VII. CONCLUSIONS

The predictive capability of a Taylor-type crystal-plasticity modeling framework, together with the phenomenological descriptions of the complex slip and

twin-hardening interactions and a new grain-fragmentation scheme, was critically evaluated by direct comparisons with experimental measurements on polycrystalline commercial-purity  $\alpha$ -titanium. Combined with our previous study on high-purity  $\alpha$ -titanium, the following conclusions are drawn.

1. The modeling framework presented for hcp metals provided reasonable predictions of the anisotropic stress-strain response and the evolution of the underlying texture during large plastic strains in  $\alpha$ -titanium. Of particular significance is the fact that the model has been validated for samples with strong initial textures that are substantially different from each other.
2. All necessary model parameters (slip and twin resistance, as well as hardening parameters) were successfully extracted from two simple compression tests performed in two different sample directions. This was possible because the sample had a substantially different initial texture with respect to the selected compression directions.
3. A comparison of the slip-system level hardening parameters extracted for the high-purity and commercial-purity grades of  $\alpha$ -Ti indicates that the impurities scale up the initial resistances of all the different families of the slip systems by a more or less a uniform scaling factor. The effect of impurities on the initial twin resistances was observed to be higher compared to the effect on the initial slip resistances. Furthermore, the impurities produced a dramatic increase in the initial hardening rates, which is attributed to the inhibition of dynamic recovery.

## ACKNOWLEDGMENTS

This work was performed while one of the authors (XW) was at Drexel University, and it was financially supported by the National Science Foundation under Grant No. DMR-0201382. The authors also thank



Professor R.D. Doherty from Drexel University for the discussions on various aspects of this study. One of the authors (AAS) gratefully recognizes the support received under the auspices of Air Force Contract No. F33615-03-D-5801.

## REFERENCES

1. X. Wu, S.R. Kalidindi, C. Necker, and A.A. Salem: *Acta Mater.*, 2007, vol. 55, pp. 423–32.
2. R.P. Singh and R.D. Doherty: *Metall. Trans. A*, 1992, vol. 23A, pp. 307–20.
3. J.W. Christian and S. Mahajan: *Progr. Mater. Sci.*, 1995, vol. 39, pp. 1–157.
4. S. Nemat-Nasser, W.G. Guo, and J.Y. Cheng: *Acta Mater.*, 1999, vol. 47, pp. 3705–20.
5. E. El-Danaf, S.R. Kalidindi, and R.D. Doherty: *Int. J. Plast.*, 2001, vol. 17, pp. 1245–65.
6. S. Mahajan and G.Y. Chin: *Metall. Mater.*, 1973, vol. 21, p. 173.
7. S. Asgari, E. El-Danaf, S.R. Kalidindi, and R.D. Doherty: *Metall. Mater. Trans. A*, 1997, vol. 28A, pp. 1781–95.
8. G.T. Gray, III: *J. Phys. IV*, 1997, vol. C3, p. 423.
9. E. El-Danaf, S.R. Kalidindi, and R.D. Doherty: *Metall. Mater. Trans. A*, 1999, vol. 30A, pp. 1223–33.
10. A.A. Salem, S.R. Kalidindi, R.D. Doherty, and S.L. Semiatin: *Metall. Mater. Trans. A*, 2006, vol. 37A, pp. 259–69.
11. R.J. Asaro: *J. Appl. Mech.*, 1983, vol. 50, pp. 921–34.
12. R.J. Asaro and A. Needleman: *Acta Metall.*, 1985, vol. 33, pp. 923–53.
13. K.K. Mathur and P.R. Dawson: *Int. J. Plast.*, 1989, vol. 5, pp. 67–94.
14. S.R. Kalidindi, C.A. Bronkhorst, and L. Anand: *J. Mech. Phys. Solids*, 1992, vol. 40, pp. 537–69.
15. M. Kothari and L. Anand: *J. Mech. Phys. Solids*, 1998, vol. 46, pp. 51–83.
16. R.A. Lebensohn, H. Uhlenhut, C. Hartig, and H. Mecking: *Acta Mater.*, 1998, vol. 46, pp. 4701–09.
17. S.R. Agnew, C.N. Tome, D.W. Brown, T.M. Holden, and S.C. Vogel: *Scripta Mater.*, 2003, vol. 48, pp. 1003–08.
18. A. Staroselsky and L. Anand: *Int. J. Plast.*, 2003, vol. 19, pp. 1843–65.
19. A.A. Salem, S.R. Kalidindi, and S.L. Semiatin: *Acta Mater.*, 2005, vol. 53, pp. 3495–3502.
20. G. Proust, C.N. Tome, and G.C. Kaschner: *Acta Mater.*, 2007, vol. 55, pp. 2137–48.
21. P.A. Turner and C.N. Tome: *Acta Metall.*, 1994, vol. 42, pp. 4143–53.
22. S.R. Agnew, P. Mehrotra, T.M. Lillo, G.M. Stoica, and P.K. Liaw: *Acta Mater.*, 2005, vol. 53, pp. 3135–46.
23. S. Balasubramanian and L. Anand: *Acta Metall.*, 2002, vol. 50, p. 133.
24. T. Mohri, M. Mabuchi, M. Nakamura, and T. Asahina: *Mater. Sci. Eng.*, 2000, vol. A290, pp. 139–44.
25. J. Koike, R. Ohyama, T. Kobayashi, M. Suzuki, and K. Maruyama: *Mater. Trans.*, 2003, vol. 44, pp. 445–51.
26. A.A. Salem, S.R. Kalidindi, and R.D. Doherty: *Acta Mater.*, 2003, vol. 51, pp. 4225–37.
27. A.A. Salem, S.R. Kalidindi, and R.D. Doherty: *Scripta Mater.*, 2002, vol. 46, pp. 419–23.
28. G.I. Taylor: *J. Inst. Met.*, 1938, vol. 62, pp. 307–24.
29. S.R. Kalidindi, A. Abusafieh, and E. ElDanaf: *Exp. Mech.*, 1997, vol. 37, pp. 210–15.
30. J.S. Kallend, U.F. Kocks, A.D. Rollett, and H.R. Wenk: *Mater. Sci. Eng.*, 1991, vol. A132, pp. 1–11.
31. A.A. Salem, S.R. Kalidindi, R.D. Doherty, M.G. Glavicic, and S.L. Semiatin: *Ti-2003 Sci. Technol.*, 2004, pp. 1429–36.
32. S.R. Kalidindi: *Int. J. Plast.*, 2001, vol. 17, pp. 837–60.
33. R.A. Lebensohn and C.N. Tome: *Acta Metall.*, 1993, vol. 41, p. 2611.